Density controlled conductivity of pristine graphene films

Azin Fahimia, Izabela Jurewicza, Ronan J. Smithb, Christopher S. Sharrocka, David A. Bradleya, Simon J. Henleyc, Jonathan N. Colemanb, Alan B. Daltona, ,

Abstract

Single or few layer graphene can be considered an exciting pseudo-two-dimensional molecular material that potentially has a wide range of applications. A critical bottleneck may arise with issues in their controlled assembly into macroscopic ensembles over large areas both in two and three dimensions. Langmuir-type assembly is a particularly useful method to control and manipulate the distribution of graphene at the air–water interface via edge–edge interactions. In this study, pristine graphene suspended in organic solvent was prepared through adaptation of a previously developed process involving the non-invasive exfoliation of graphite. Successful deposition of graphene at the air–water interface was achieved by manipulating the vapor-pressure of the graphene dispersion through solvent mixing. Through careful control of density, by following the pressure-area isotherm during monolayer compression, it is possible to precisely tune the electrical conductivity. The resulting assemblies can be easily transferred to glass and other substrates using the Langmuir–Schaefer horizontal deposition method producing thin films with tunable electrical conductivity that exhibits percolation-type behavior. A major advantage of this process is that the conducting films require no further treatment unlike their graphene-oxide counterparts. Moreover, the physical properties of these assemblies can be easily controlled which is a precursor for graphene-based electronic applications.

1. Introduction

Graphene, a two-dimensional (2D) honeycomb lattice structure of carbon atoms, possesses intriguing properties. It's micrometer-scale ballistic-type electrical transport [1] and [2] opens up the possibility for many new applications such as field-effect [3] and spintronic devices [4] as well as chemical sensing [5]. It's intrinsic strength, modulus [6] as well as thermal conductivity [7] far exceeding that of diamond [8] or carbon nanotubes (CNTs) [9] has inspired the fabrication of high-performance functional composite materials [10] and [11] and electronic circuits [12] and [13]. However to fully utilize graphene's unique properties there are two bottlenecks to overcome; namely (i) the controlled production of high-quality graphene with a selected number of layers in large quantities and (ii) the controlled uniform deposition of graphene over large areas.

Several methods have been developed to produce high quality graphene including micromechanical cleavage [14], epitaxial growth [15] and [16], chemical reduction of exfoliated graphene oxide [17], [18] and [19], chemical vapor deposition (CVD) growth [20] and liquid phase exfoliation of graphite [21]

and [22]. However, only the latter method appears to be, at present, suited for mass production of high-quality un-oxidized graphene that can be fully dispersed in a wide variety of organic solvents [23]. Good control over the chemical purity of the sheets is essential for the efficiency of graphene-based electronic devices and sensors, and different approaches to achieve this have been reported. Mono- or multilayers of 2D pristine graphene and graphene oxide (GO), can be assembled from solution using conventional layer-by-layer (LbL) assembly [24], [25], [26] and [27], at liquid–liquid interfaces [46], by vacuum filtration [28] and [29], or by spray coating [23].

The assembly of materials at the air–water interface using the Langmuir process is another way of fabricating thin films. It can be realized by spreading a dispersion which has been previously dispersed in an organic solvent onto a water subphase, evaporating the solvent and finally compressing the floating monolayer. The vertical or horizontal transfer to a substrate can be achieved using the Langmuir–Blodgett (LB) [17], [30], [31] and [32] or the Langmuir–Schaefer (LS) [33] techniques respectively. The LB and LS methods facilitate the formation of thin films with controlled thickness and a high degree of structural order. There have been several reports already of using these techniques to produce films of GO, which can then be thermally or chemically treated to form graphene. However the need for this final step is not ideal [31], [17] and [33].

Here we show a method to produce pristine graphene thin films using the LS approach which requires no post-processing treatment. Typically, solvents that have been shown to efficiently exfoliate graphene have low vapor pressure and are hence not ideal for use in the LS process. We therefore use a mixed solvent strategy which not only facilitates efficient liquid phase exfoliation of graphene but modification to the solvent mass ratio manipulates the vapor pressure so as to be more amenable for the process. The resulting dispersions can be successfully used as a pre-cursor to the self-assembly of pristine graphene at the air–water interface which can be subsequently transferred by the LS technique onto a solid substrate. The technique allows for the deposition of pristine graphene flakes over large areas and for control over film density as well as the number of layers in the film. Through careful control of density, by following the pressure-area isotherm during monolayer compression, it is possible to precisely tune the electrical conductivity. Our results point to the potential of the LS deposition technique to prepare high quality graphene films on various substrates which potentially could be suitable for a range of applications including thin-film flexible electronics, optoelectronics and sensors.

2. Experimental methods

2.1. Graphene dispersion

The graphene dispersion was prepared as described elsewhere [22]. Briefly, as-produced sieved graphite powder (Aldrich product 332461, batch number 06106DE) was added to N-methylpyrrolidone (NMP) (spectrophotometric grade, 99.0%) to give an initial graphitic concentration of 0.1 mg/ml. This mixture was sonicated using low power bath sonication (Model Ney Ultrasonic) for 30 min. The resulting dispersion was then centrifuged (using a Hettich Mikro 22R centrifuge) for 90 min at 500 rpm. The resulting supernatant was used for further processing. The final dispersed graphene concentration in NMP was calculated to be 0.0876 mg/ml (from the absorbance at 660 nm using an extinction coefficient of 3620 L/g/m). 1 ml of the resulting NMP dispersion was mixed with 100 ml of chloroform (Sigma Aldrich) and sonicated using bath sonicator (fisher scientific FB15051) for 60 min, followed by centrifugation (Eppendorf 5702) for 90 min at 4000 rpm–2500 G. The supernatant was then bath sonicated under chilled conditions (ice bath) for a further 30 min. The final dispersed graphene concentration in NMP/chloroform mixture was calculated to be 0.007 mg/ml.

2.2. Langmuir–Schaefer (LS) deposition of graphene

For LS deposition of graphene, a commercial NIMA deposition trough (NIMA technology, model 612D) was used. In order to form a monolayer at the air–water interface, the graphene dispersion in a chloroform/NMP mixture (8–10 ml) was spread onto the water subphase (ultra-pure Millipore water) with a microliter syringe utilizing drop-by-drop deposition technique. The pressure-area isotherms were obtained after 10 min waiting time to let the remaining solvent evaporate. The surface tension was determined by suspending a Wilhelmy paper plate completely wetted by water, and measuring the downward force on it during compression of the monolayer by moving two opposing barriers towards each other at the speed of 15 cm2/min. Thin films of graphene were then transferred onto glass substrates by LS horizontal deposition technique at various surface pressures (ranging from 0 to 40 m N/m) using a transfer speed of 3 mm/min. Prior to the film deposition, substrates were cleaned by rinsing them thoroughly with deionised water followed by sequential sonication in deionised water, isopropyl alcohol (IPA) and methanol for 5 min in each solvent.

2.3. Characterization

The length distribution of graphene flakes in NMP was evaluated statistically using a transmission electron microscopy (TEM) by drop casting the dispersion onto a holey carbon TEM grid. The length distribution of graphene in NMP/chloroform mixture as well as thickness distribution of graphene flakes in both, NMP and NMP/chloroform was evaluated statistically using an Atomic Force Microscopy (AFM). Samples were prepared by spin-coating the dispersion onto freshly cleaved mica at 3000 rpm for 10 s. Atomic Force Microscopy (AFM) topographic analysis of the dispersions as well as LS graphene films deposited on glass substrates was performed in a semi-contact mode using NT-MDT AFM

(Moscow, Russia). The AFM probes used (NT-MDT) had an average spring constant of 11.8 N/m.

The current–voltage characteristics have been obtained using a Keithley Model 4200. The final specific conductivity as calculated from the resistance and thickness of the film. All sample thicknesses were measured using AFM. Gold electrodes ~70 μm thick were evaporated using Kurt J. Lesker evaporator on top of LS graphene films. The distance between electrodes was 4 mm. The width (W) and length (L) of each electrode was 1 and 8 mm respectively. The transmittance data of LS films was obtained by UV–VIS/NIR spectrophotometer (Cary 5000).

3. Results and discussion

3.1. Dispersion and exfoliation of graphene in high and low boiling point solvents

The graphene dispersion in N-methyl-pyrrolidone (NMP) has been prepared by the method of liquid phase exfoliation of graphite [22]. The choice of solvent was dictated by its ability to achieve suspensions of high quality, defect-free, and un-oxidized graphene at relatively high concentrations [34]. Histograms of the size distribution of flakes as obtained from TEM analysis are shown in Fig. 1. As can be seen, graphite is almost completely exfoliated to multilayer structures with less than 5 layers in NMP. The average flake size is 500 nm. Representative TEM images of the flakes observed are shown in Fig. 1b where graphene monolayers (with well-defined edges) as well as multilayers can be easily distinguished. It should be noted that a small number of larger objects (a few tens of flakes thick) was also present in the dispersion. The high dispersion efficiency of NMP is attributed to its ability to match the surface energy of graphene. Consequently, the NMP–graphene interaction is balanced with the exfoliation energy resulting in a minimal energy cost to overcome van der Waals forces between the graphene flakes [22] and [35].

Fig. 1.

(a) Histogram of the number of visual observations of flakes as a function of the number of monolayers per flake for NMP dispersions obtained from TEM analysis (inset: optical photograph of the high concentration graphene dispersion in NMP) and (b) representative TEM micrographs showing well exfoliated graphene flakes in NMP. (c) Size distribution (inset of 1c: optical photograph of the low concentration graphene dispersion in NMP/chloroform mixture) and (d) thickness histograms of graphene flakes deposited from NMP/chloroform mixture (inset of 1d: representative AFM topography image of a single layer graphene flake and its height profile).
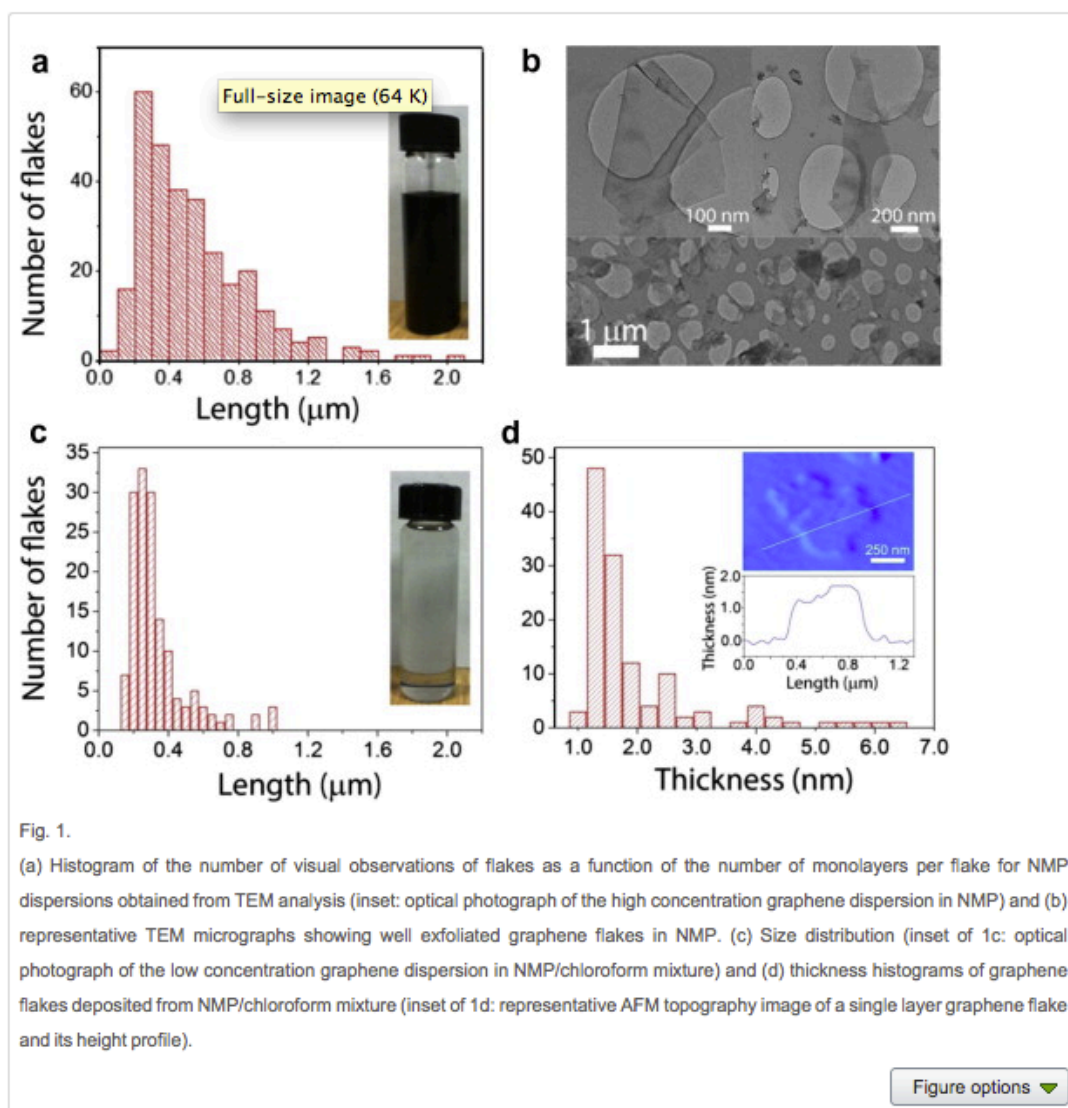
Figure options ▼

Fig. 1.

Since NMP is completely miscible with chloroform [36], the initial graphene dispersion was diluted down to a ratio (NMP/chloroform) of 1:100 as described in the experimental section. To estimate the size distribution of graphene flakes after dilution, AFM analysis was performed and histogram analysis of length (Fig. 1c) and thickness (Fig. 1d) of more than 150 graphene flakes were obtained. It can be seen that a large population of flakes are single-layered as shown on the representative AFM topography image and height profile in the inset of Fig. 1d. However, flakes consisting of two-layers, three layers and multilayers are also present. The average flake major axis is ~305 nm which is smaller than those observed in the initial NMP dispersion. Narrowing of the flakes length distribution as well as the thickness maybe due to further dilution and additional ultracentrifugation of the already exfoliated flake [37].

The use of the NMP/chloroform mixture to facilitate the spreading process is not a new concept, and has been successfully used previously for the deposition of conducting polymers [38] and [39]. Such a mixed-solvent strategy is required for

the following reasons. Firstly, the LS deposition technique requires the use of a low boiling point, water immiscible solvent. This is because the spreading solvent must evaporate within a reasonable period of time to avoid residue being present in the condensed material [40] and [41]. NMP is highly miscible with water and its vapor pressure at 20 °C is very low so, on its own, is inappropriate for the deposition of graphene. When a nonvolatile solute such as NMP is added to a volatile solvent such as chloroform, the vapor pressure of the solution will be lower than that of the pure solvent as determined by Raoult's Law. The vapor pressure of chloroform and NMP at room temperature is 21.3 and 0.039 kPa, respectively. The total vapor pressure will lie between the vapor pressures of the pure components, and can be determined by the mixture composition according to the following formula [42]:

$$ P_{\text{mixture}} = P_A^\circ X_A + P_B^\circ X_B $$

where View the MathML source and View the MathML source are the partial pressures and XA and XB are the mole fractions of the component A and B respectively. As can be seen in Fig. 2, the addition of chloroform to the significantly increases the vapor pressure (from 0.039 to 21.04 kPa) while having little effect on dispersion quality.

Fig. 2.

(a) The total vapor pressure of the NMP/chloroform mixture calculated using Raoult's law.

Figure options

A dilution of the graphene dispersion in the solvent mixture also enables complete spreading of graphene over the interface. The use of a more concentrated graphene dispersion results in poor spreading due to large graphene flakes being hindered from accessing the water surface. If a dilute solution is used, the monolayer is laterally homogeneous and the isotherms are independent of spreading conditions, compression speed and are nearly free of hysteresis.

Fig. 2.

(a) The total vapor pressure of the NMP/chloroform mixture calculated using Raoult's law.

Figure options ▼
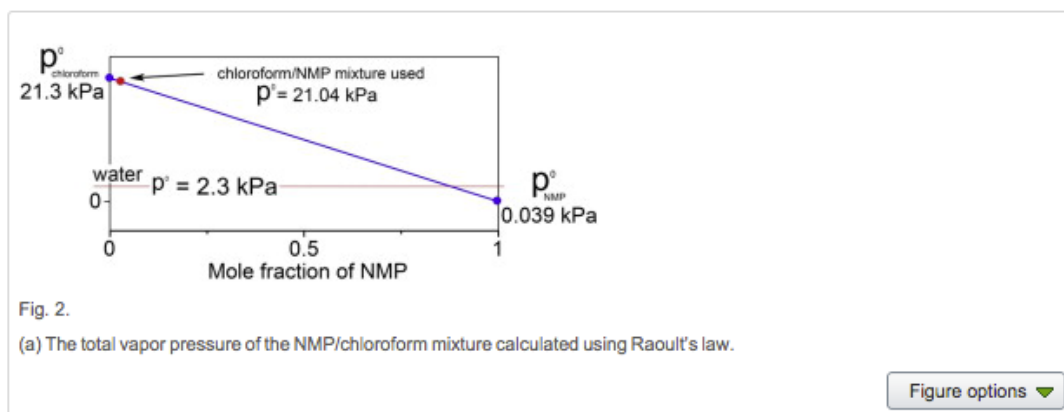
The presence of a small amount of NMP is also critical. As shown by O'Neill et al. [23] the dispersion and exfoliation of graphene in solvents can be predicted by using the Hansen solubility parameters (HSP) consisting of a dispersion force component (δD), a polar component (δP) and a hydrogen bonding component (δH). Good quality graphene dispersions can only be achieved for solvents that possess HSPs matching well with those for graphene [23]. Chloroform is one of the least successful solvents, probably due to its polar component δP = 3.1 (MPa)1/2 which is located at the edge of the acceptable values for solubilization of graphene (3–17 MPa1/2). It is widely accepted that the HSP for a solvent mixture is a linear function of composition [43] according to the following formula:

$$\delta\text{mixture} = \Sigma_{\phi}\text{n,comp}_{\delta}\text{n,comp}$$

where ϕ is the volume fraction for each solvent present. Therefore, due to presence of NMP in chloroform, HSPs are shifted towards greater graphene solubility. The resulting dispersion is stable with no precipitation occurring even after a week (inset of Fig. 1c).

3.2. Spreading of graphene films at the air–water interface

As water has a high surface tension at room temperature, when a solution of graphene dispersed in a water-insoluble solvent such as chloroform is placed on the surface, it rapidly spreads to cover the available area. During solvent evaporation, graphene sheets tend to assemble into 2D films. If the graphene concentration per unit area is low, the distance between adjacent graphene flakes is large and their interactions are weak. At this point, the monolayer can be regarded as a 2D gas that has one interface with the aqueous phase and the other with air and thus has little effect on the surface tension.

When the available surface area of the monolayer is reduced by moving a barrier across the water surface, the graphene flakes start to exert a repulsive force on each other initiating a reduction in surface tension. During compression, the monolayer undergoes phase transitions from gas to liquid to solid phases before collapsing, yielding a surface pressure-surface area (density) (Π-A) isotherm. A typical Langmuir compression isotherm of a graphene monolayer is shown in Fig. 3 with distinct phase changes and a collapse pressure above 39 m N/m.

Fig. 3.

(a) Representative surface pressure-area (Π-A) isotherm of graphene monolayer deposited from chloroform/NMP mixture at the air–water interface. (b) A corresponding photograph of a Langmuir trough showing a dense graphene monolayer with a glass substrate above the surface ready for a Langmuir–Schaefer deposition.

Fig. 3.

(a) Representative surface pressure-area (Π-A) isotherm of graphene monolayer deposited from chloroform/NMP mixture at the air–water interface. (b) A corresponding photograph of a Langmuir trough showing a dense graphene monolayer with a glass substrate above the surface ready for a Langmuir–Schaefer deposition.
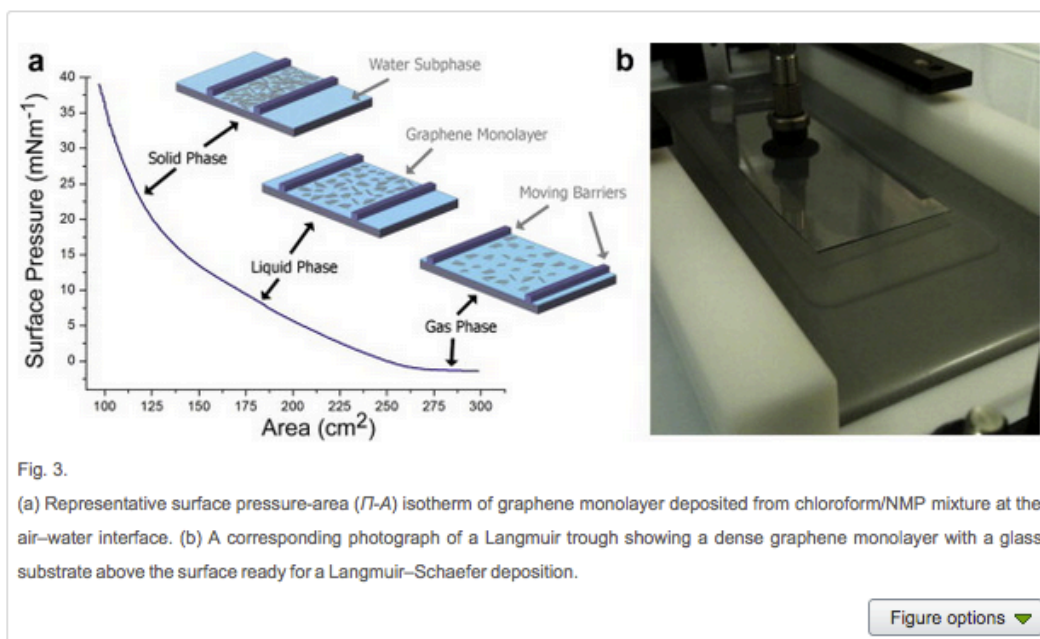
A compressed graphene monolayer can be considered to be a 2D solid film that is strong and rigid and does not exhibit typical monolayer collapse behavior normally associated with Langmuir prepared monolayer such as lipids. As can be seen in the photographs in Fig. 4 taken perpendicular to the optical axis, the packing density of graphene flakes can be manipulated by altering the surface pressure during the compression/expansion cycle. At a Π = 0 m N/m, graphene flakes are separated from each other forming multiple discrete monolayer islands of various sizes with a surface of a few μm2. The presence of these islands is probably a consequence of the large volume of graphene dispersion deposited (10 ml). At lower volumes (below 5 ml), the graphene monolayer is not visible on the water subphase and is difficult to investigate optically until large surface pressures are reached. By compressing the barriers, the monolayer is densified resulting in the multiple discrete islands becoming connected and thus reducing the free space. Compression of the film up to the Π = 40 m N/m results in merging of the monolayer islands into a continuous closely packed monolayer.
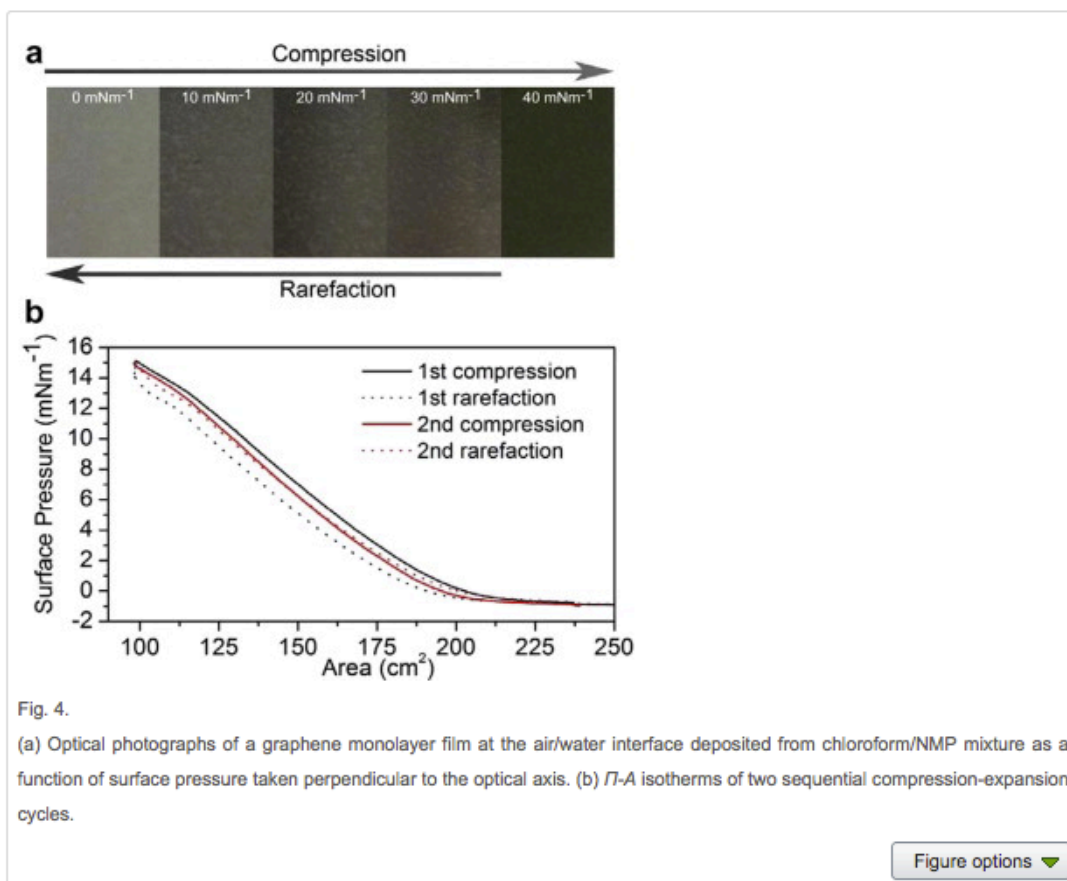
Fig. 4.

(a) Optical photographs of a graphene monolayer film at the air/water interface deposited from chloroform/NMP mixture as a function of surface pressure taken perpendicular to the optical axis. (b) Π-A isotherms of two sequential compression-expansion cycles.

Fig. 4.

(a) Optical photographs of a graphene monolayer film at the air/water interface deposited from chloroform/NMP mixture as a function of surface pressure taken perpendicular to the optical axis. (b) Π-A isotherms of two sequential compression–expansion cycles.

Figure options ▼

It should be noted that the interfacial area can only be reduced to a point where graphene flakes resist packing into a higher density state due to the hard limit dictated by the molecular cross-sectional area. Further compression from this point compromises the stability of the interface and leads to film collapse defined as the movement of graphene flakes from the interface into the bulk resulting in their transition to an out-of-plane geometry (see Supporting information Fig. S1).

It is possible to reversibly tune the density if the target surface pressure is not more than 25 m N/m. For example, Π-A isotherms of two sequential compression-expansion cycles (0–15 m N/m) are shown in Fig. 4b and as a Video S1 in the supporting information. During the first compression–rarefaction cycle, a minor degree of hysteresis was observed, but this effect was essentially absent during further recompression. Typically, the monolayers formed contain graphene flakes of various thicknesses ranging from single layered graphene to multilayered structures. Due to the variation in thicknesses, they are not able to overlap, leading to reversible density alterations of the monolayers during several compression/expansion cycles. It is likely that the presence of a negligible amount of residual NMP also aids the spreading by acting as a "molecular lubricant", which is slowly squeezed out under applied surface pressure and assists in the increased reversibility of the monolayers during repetitive compression/expansion cycles. The reversibility has also been observed by Cote et al. [31] for GO deposited onto a water subphase from a

water/methanol mixture. However, in their situation it is due to the presence of electrostatic repulsion between adjacent flakes.

3.3. Langmuir–Schaefer deposition of graphene monolayer films

The LS technique is used to transfer graphene monolayers from the air/water interface onto a solid substrate. When the graphene monolayer is spread onto the water and compressed to a desired density the substrate is lowered onto the graphene covered interface. Once contact is made the substrate is then retracted resulting in the graphene monolayer being transferred onto the substrate. The choice of LS method over LB was dictated by the fact that LS is more appropriate for the transfer of highly rigid monolayers because the floating monolayer is subjected to less disruptive forces than in the LB method [41].

Fig. 5a shows a representative AFM height image of a dense graphene film deposited from the maximum surface pressure of ~40 m N/m which is just before the point of monolayer collapse. The transferred film is homogenous and free of microscopic voids over its entire area. The line profile in Fig. 5b along the yellow horizontal line in Fig. 5a shows a modal average thickness of ~5 nm.

Fig. 5.

(a) A representative AFM topography image of highly dense Langmuir–Schaefer film deposited at Π = 40 m N/m. This film has a transmittance (@550 nm) of 84.3% (b) the corresponding line profile taken at the horizontal yellow line denoted in Fig. 5a. (For interpretation of the references to colour in this figure legend, the reader is referred to the web version of this article.)

Fig. 5.

(a) A representative AFM topography image of highly dense Langmuir–Schaefer film deposited at $\Pi = 40$ m N/m. This film has a transmittance (@550 nm) of 84.3% (b) the corresponding line profile taken at the horizontal yellow line denoted in Fig. 5a. (For interpretation of the references to colour in this figure legend, the reader is referred to the web version of this article.)

Figure options ▼
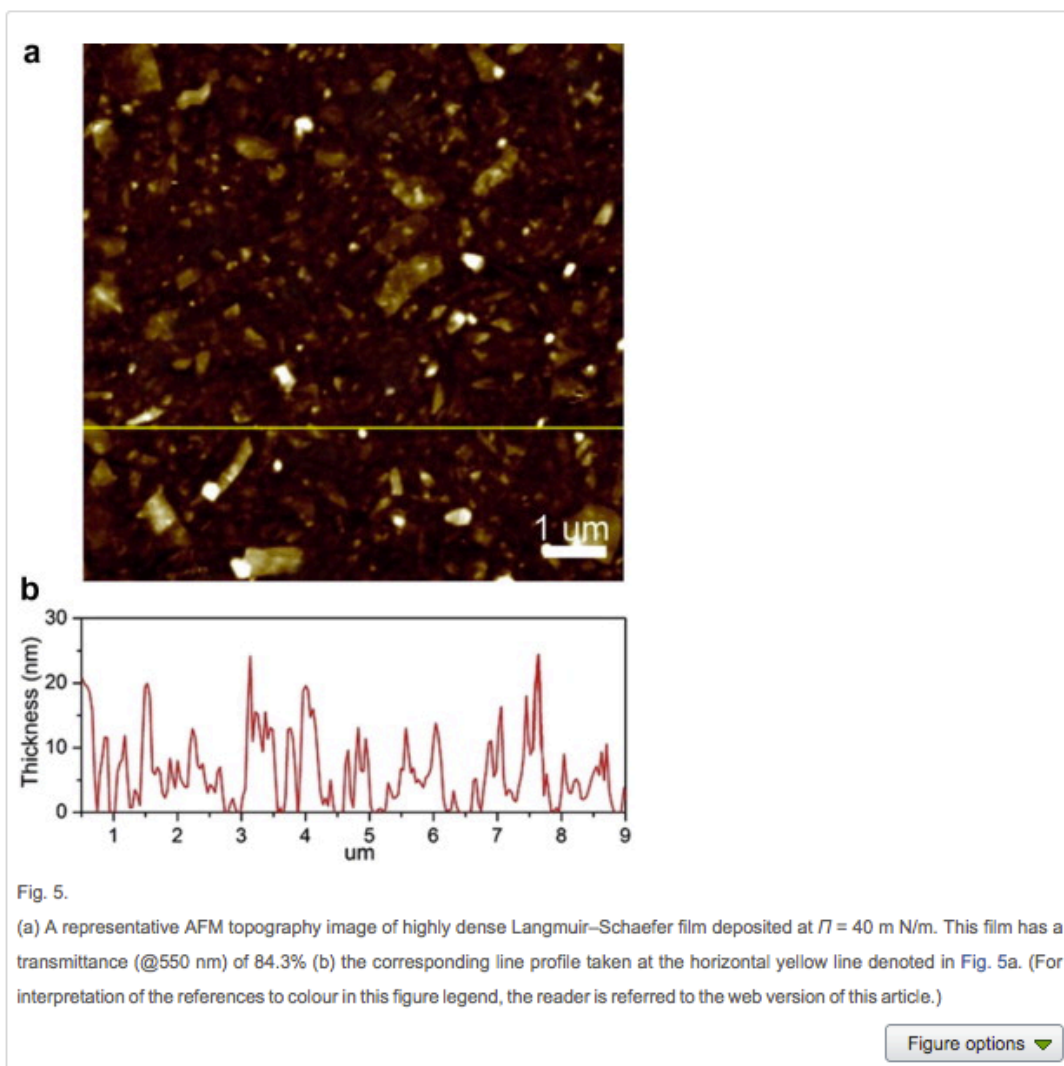
By following the Π-A isotherm, monolayers at different surface pressure ranging from 0–40 m N/m deposited on glass substrates are shown in Fig. 6a–e. A film deposited from the gas phase (at Π = 1 m N/m) is low in density and contains large voids. The deposition at higher Π results in the formation of denser films and consequently fewer voids, until the maximum surface coverage is reached at ~40 m N/m.

Fig. 6.

AFM topography images of graphene flakes deposited by the Langmuir–Schaefer technique from NMP/chloroform mixture as a function of surface pressure (a) 1, (b) 10, (c) 20, (d) 30 and (e) 40 m N/m.

Fig. 6.

AFM topography images of graphene flakes deposited by the Langmuir–Schaefer technique from NMP/chloroform mixture as a function of surface pressure (a) 1, (b) 10, (c) 20, (d) 30 and (e) 40 m N/m.

Figure options ▼
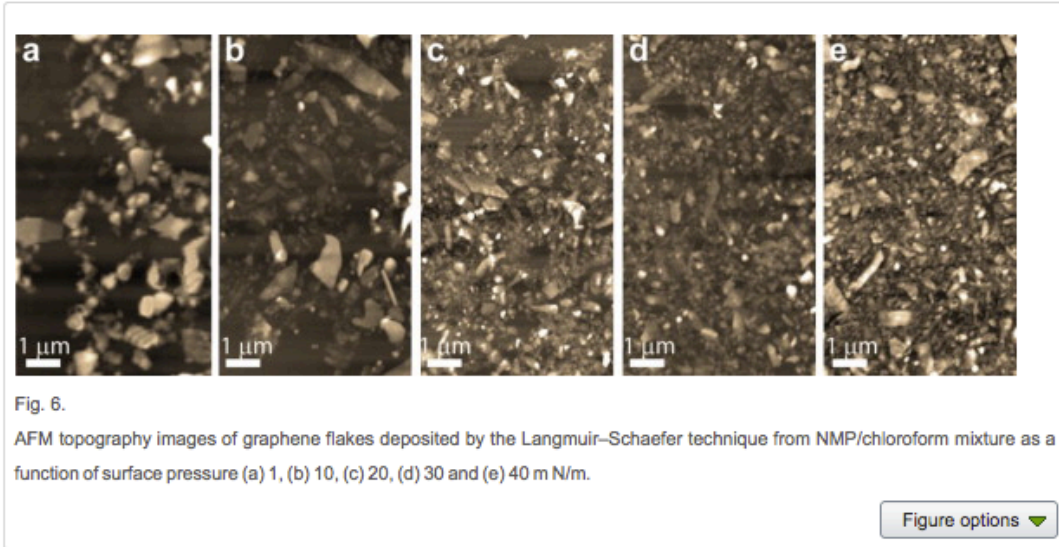
## 3.4. Electrical properties of Langmuir graphene films

While the resulting films are electrically conducting, the absolute conductivity depends on the density of graphene which is controlled by the Langmuir process. In order to analyze this dependence the surface coverage as a function of Π can be obtained directly by processing AFM height images using ImageJ software as shown in Fig. 7a and in the Supporting information Fig. S2. Here, the black regions represent the substrate, while white regions represent the graphene flakes. The electrical conductivity of the growing graphene islands at increased surface coverage can be analyzed using percolation theory given by:

$$\sigma = \sigma_0 (S - S_c)^t, \quad S > S_c$$

where S is the occupation probability of a conducting area on the substrate (also known as fractional coverage), Sc is the critical value of fractional coverage, and t is the critical exponent of the electrical conductivity. In such networks, the ability for electrons to flow requires the formation of conductive pathways through the material. This, in turn, requires a critical density of connections for effective passage of current. As can be seen in Fig. 7b, when the surface coverage reaches ~20% the graphene flakes form islands consisting of loosely packed flakes linked by a small set of inter-cluster connections. As this stage the percolation is dominated by tunneling of charge carriers from one flake to another and the surface coverage is insufficient to allow the formation of fully-connected pathways. As the surface coverage increases, the film conductivity also increases due to the inter-flake distance reducing until one approaches 100% coverage at which point the conductivity mechanism is ohmic in behavior (as evidenced by I-V characteristics). The best-fitting curve to the data using percolation-type power law scaling is shown in Fig. 7b yielding a critical exponent t = 8.95, a conductivity coefficient σ0 = 46 S/m and a formation of the percolative network at Sc = 9% respectively. Such a high value of a critical exponent t has been previously reported and may be associated with the large distribution of junction resistances at flake–flake interfaces [44].

Fig. 7.

(a) The change in the electrical conductivity as a function of surface coverage (inset: electrical conductivity as a function of number of layers deposited). (b) Thresholded AFM images of LS films as a function of pressure showing the change in packing density (here the black areas show the background while the white areas represent the graphene flakes).


Fig. 7.

(a) The change in the electrical conductivity as a function of surface coverage (inset: electrical conductivity as a function of number of layers deposited). (b) Thresholded AFM images of LS films as a function of pressure showing the change in packing density (here the black areas show the background while the white areas represent the graphene flakes).

Figure options ▼
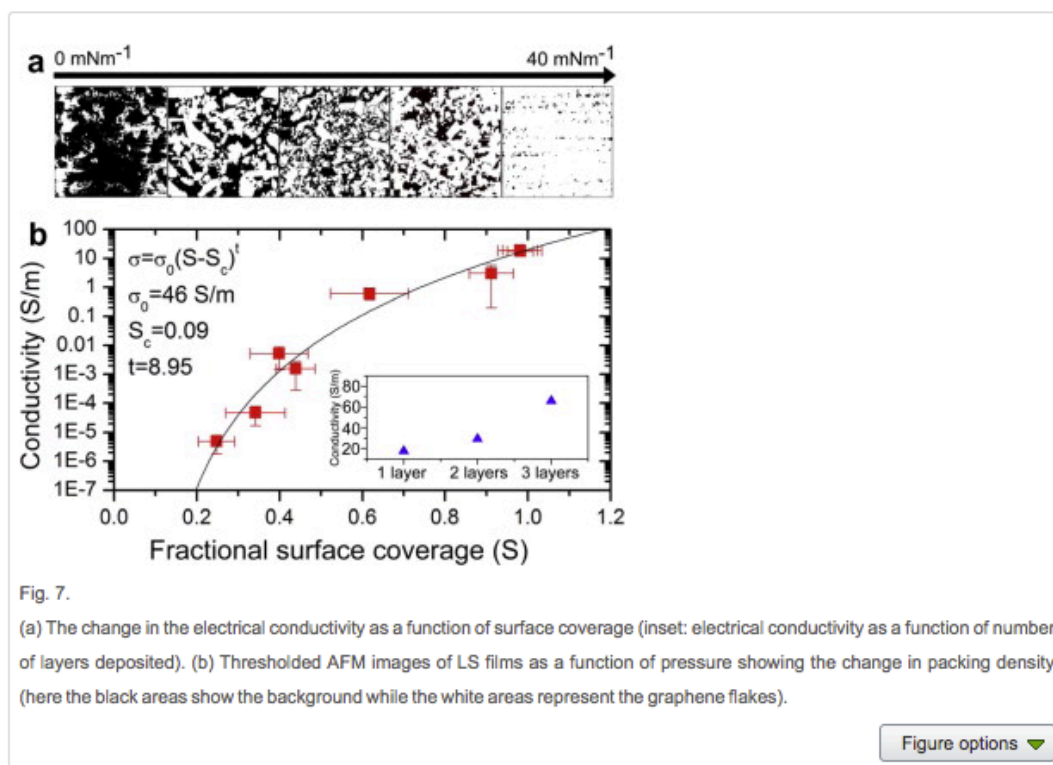
The highest conductivity for a 1 layer thin film of graphene obtained by LS is ~19 S/m which is expectedly low compared to the intrinsic conductivity of the individual graphene flakes. Since, the films produced consist of graphene flakes of varying thickness, as observed by AFM, the broad distribution of their thicknesses requires charge transport parallel and perpendicular to the graphene sheets. As reported by Nirmalraj et al. [45], the interflake resistance is linearly dependent on the graphene thickness. They showed, by connecting a monolayer graphene flake with a bi-layer graphene the resistance at the intersection of ~550–650 Ω was measured. However, when a monolayer graphene was connected to the tri-layer graphene, the resistance jump at the intersection was as high as ~6.5 kΩ.

Repetitive stamping of a substrate on the floating monolayer enables the formation of thicker films. As shown in the inset of Fig. 7b, bi-layers and triple-layered films deposited at the highest surface pressure of ~40 m N/m yield a conductivity of ~30 and ~65 S/m respectively. The conductivity can be further enhanced by increasing the number of layers however the transparency would have to be sacrificed.

Since the film's transmittance is strongly dependent on the graphene density, it decreases exponentially as the conductivity increases as shown in Fig. 8. One layer of graphene with a conductivity of ~4.8 × 10−6 S/m has a 95% transmittance, while a graphene film of the highest density has a conductivity almost four times higher (~19 × 10−6 S/m) while the transmittance is lowered by only ~10%. Additionally, for highly dense graphene films it is possible to tune the conductivity without significantly sacrificing their transmittance.

Fig. 8.

Transmittance versus conductivity for monolayer graphene films.

Fig. 8.

Transmittance versus conductivity for monolayer graphene films.

Figure options ▼
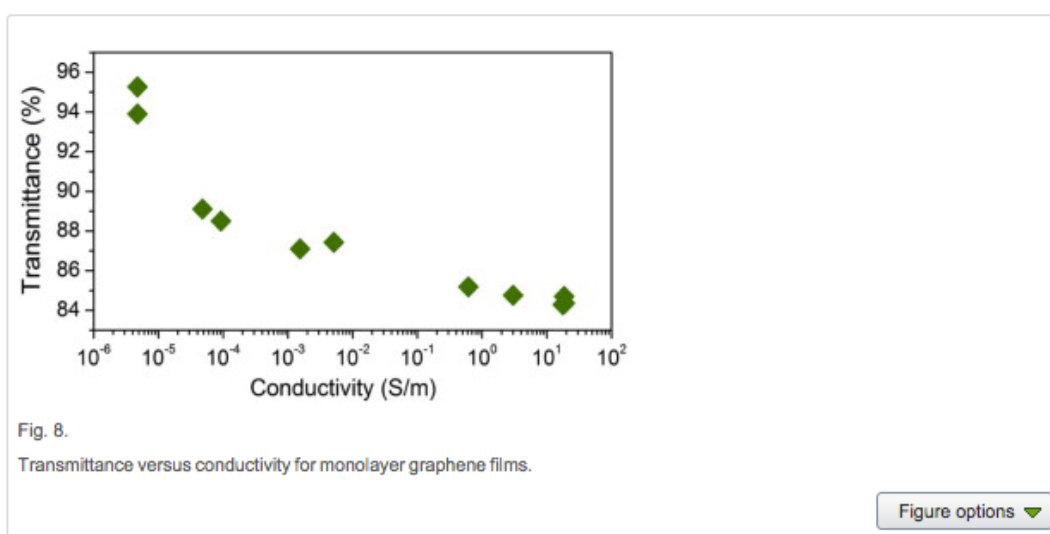
The above results point to the process as being ideally suited to the preparation of large area electrically conducting graphene assemblies. We have shown that the transfer of the films formed at the air–water interface to solid substrates is simple and results in solid films of reproducible physical properties. Unlike GO thin films our systems require no further chemical or thermal treatment to produce electrically conducting arrays. Interestingly, the controlled deposition of such conducting assemblies at the air–water interface may have a range of applications in their own right without transfer to a substrate. For instance, differences in the extent of protonation on either side of water–hydrophobe interfaces are deemed essential to enzymatic catalysis, molecular recognition, bioenergetic transduction, and atmospheric aerosol–gas exchanges and could be easily measured using our floating graphene electrodes. Another application that these films would be ideally suited to is to understand the role the ocean plays in the biochemical cycles of climate modifying gases such as carbon dioxide. The influence of monomolecular films on the gas exchange process is essential. The graphene layers could be used as proxies for biogenic slicks which are prevalent to coastal waters and gas exchange rates could be better determined by dynamically measuring changes in conductivity which we are currently investigating (see Supporting information Fig. S3 for preliminary results).

4. Conclusion

We have successfully demonstrated assembly of pristine graphene at the air–water interface. The resulting water-supported monolayers can be made by deposition from solvent mixtures with controlled vapor-pressure. The edge-to-edge repulsion between the layers prevented them from overlapping during compression which is facilitated by the presence of small quantities of a high boiling point solvent NMP. The monolayers respond pseudo-elastically to compression and rarefaction with little hysteresis. The resulting monolayers can be readily transferred to a solid substrate with density continuously tunable from dilute, close-packed to over-packed monolayers of interlocking sheets using the Langmuir–Schaeffer method. The resulting deposited films are electrically conducting with absolute conductivity controlled by the preparation process. Most importantly, unlike similar films prepared using GO the films require no further treatment with their electrical conductivity defined by the inter-layer junction resistance. Moreover, multi-layer films can be prepared by consecutive layer by layer assembly. The study shows that the LS technique is a simple but effective method to prepare macroscopic films of pristine graphene with controlled physical properties which is a precursor for graphene-based electronic applications.

REFERENCES

[1] Chen J-H, Jang C, Xiao S, Ishigami M, Fuhrer MS. Intrinsic and extrinsic performance limits of graphene devices on SiO_2. Nat Nanotechnol 2008;3(4):206–9.

[2] Morozov SV, Novoselov KS, Katsnelson MI, Schedin F, Elias DC, Jaszczak JA, et al. Giant intrinsic carrier mobilities in graphene and its bilayer. Phys Rev Lett 2008;100(1):016602.

[3] Vicarelli L, Vitiello MS, Coquillat D, Lombardo A, Ferrari AC, Knap W, et al. Graphene field-effect transistors as room-temperature terahertz detectors. Nat Mater 2012;11(10):865–71.

[4] Pesin D, MacDonald AH. Spintronics and pseudospintronics in graphene and topological insulators. Nat Mater 2012;11(5):409–16.

[5] Rumyantsev S, Liu G, Shur MS, Potyrailo RA, Balandin AA. Selective gas sensing with a single pristine graphene transistor. Nano Lett 2012;12(5):2294–8.

[6] Lee C, Wei X, Kysar JW, Hone J. Measurement of the elastic properties and intrinsic strength of monolayer graphene. Science 2008;321(5887):385–8.

[7] Balandin AA, Ghosh S, Bao W, Calizo I, Teweldebrhan D, Miao F, et al. Superior thermal conductivity of single-layer graphene. Nano Lett 2008;8(3):902–7.

[8] Wei L, Kuo PK, Thomas RL, Anthony TR, Banholzer WF. Thermal conductivity of isotopically modified single crystal diamond. Phys Rev Lett 1993;70(24):3764–7.

[9] Kim P, Shi L, Majumdar A, McEuen PL. Thermal transport measurements of individual multiwalled nanotubes. Phys Rev Lett 2001;87(21):215502.

[10] Wajid AS, Ahmed HST, Das S, Irin F, Jankowski AF, Green MJ. High-performance pristine graphene/epoxy composites with enhanced mechanical and electrical properties. Macromol Mater Eng 2013;3(3):339–47.

[11] Shahil KMF, Balandin AA. Graphene-multilayer graphene nanocomposites as highly efficient thermal interface materials. Nano Lett 2012;12(2):861–7.

[12] Yan Z, Liu G, Khan JM, Balandin AA. Graphene quilts for thermal management of high-power GaN transistors. Nat Commun 2012;3:827.

[13] Ghosh S, Calizo I, Teweldebrhan D, Pokatilov EP, Nika DL, Balandin AA, et al. Extremely high thermal conductivity of graphene: prospects for thermal management applications in nanoelectronic circuits. Appl Phys Lett 2008;92(15):151911.

[14] Novoselov KS, Geim AK, Morozov SV, Jiang D, Zhang Y, Dubonos SV, et al. Electric field effect in atomically thin carbon films. Science 2004;306(5696):666–9.

[15] Rubio-Roy M, Zaman F, Hu Y, Berger C, Moseley MW, Meindl JD, et al. Structured epitaxial graphene growth on SiC by selective graphitization using a patterned AlN cap. Appl Phys Lett 2010;96(8):082112.

[16] Berger C, Song Z, Li X, Wu X, Brown N, Naud C, et al. Electronic confinement and coherence in patterned epitaxial graphene. Science 2006;312(5777):1191–6.

[17] Li X, Zhang G, Bai X, Sun X, Wang X, Wang E, et al. Highly conducting graphene sheets and Langmuir–Blodgett films. Nat Nanotechnol 2008;3(9):538–42.

[18] Tung VC, Allen MJ, Yang Y, Kaner RB. High-throughput solution processing of large-scale graphene. Nat Nanotechnol 2009;4(1):25–9.

[19] Chua CK, Ambrosi A, Pumera M. Graphene oxide reduction by standard industrial reducing agent: thiourea dioxide. J Mater Chem 2012;22(22):11054–61.

[20] Kim KS, Zhao Y, Jang H, Lee SY, Kim JM, Kim KS, et al. Large-scale pattern growth of graphene films for stretchable transparent electrodes. Nature 2009;457(7230):706–10.

[21] Coleman JN. Liquid-phase exfoliation of nanotubes and graphene. Adv Funct Mater 2009;19(23):3680–95.

[22] Hernandez Y, Nicolosi V, Lotya M, Blighe FM, Sun Z, De S, et al. High-yield production of graphene by liquid-phase exfoliation of graphite. Nat Nanotechnol 2008;3(9):563–8.

[23] O'Neill A, Khan U, Nirmalraj PN, Boland J, Coleman JN. Graphene dispersion and exfoliation in low boiling point solvents. J Phys Chem C 2011;115(13):5422–8.

[24] Zeng G, Xing Y, Gao J, Wang Z, Zhang X. Unconventional layer-by-layer assembly of graphene multilayer films for enzyme-based glucose and maltose biosensing. Langmuir 2010;26(18):15022–6.

[25] Liu Y, Liu Y, Feng H, Wu Y, Joshi L, Zeng X, et al. Layer-by-layer assembly of chemical reduced graphene and carbon nanotubes for sensitive electrochemical immunoassay. Biosens Bioelectron 2012;35(1):63–8.

[26] Lu J, Liu W, Ling H, Kong J, Ding G, Zhou D, et al. Layer-by-layer assembled sulfonated-graphene/polyaniline nanocomposite films: enhanced electrical and ionic conductivities, and electrochromic properties. R Soc Chem Adv 2012;2(28):10537–43.

[27] Park JS, Cho SM, Kim W-J, Park J, Yoo PJ. Fabrication of graphene thin films based on layer-by-layer self-assembly of functionalized graphene nanosheets. ACS Appl Mater Interfaces 2011;3(2):360–8.

[28] Zhang S, Li Y, Pan N. Graphene based supercapacitor fabricated by vacuum filtration deposition. J Power Sources 2012;206:476–82.

[29] Chen H, Müller MB, Gilmore KJ, Wallace GG, Li D. Mechanically strong, electrically conductive, and biocompatible graphene paper. Adv Mater 2008;20(18):3557–61.

[30] Kulkarni DD, Choi I, Singamaneni SS, Tsukruk VV. Graphene oxide–polyelectrolyte nanomembranes. ACS Nano 2010;4(8):4667–76.

[31] Cote LJ, Kim F, Huang J. Langmuir–Blodgett assembly of graphite oxide single layers. J Am Chem Soc 2008;131(3):1043–9.

[32] Szabó T, Hornok V, Schoonheydt RA, Dékány I. Hybrid Langmuir–Blodgett monolayers of graphite oxide nanosheets. Carbon 2010;48(5):1676–80.

[33] Gengler RYN, Veligura A, Enotiadis A, Diamanti EK, Gournis D, Józsa C, et al. Large-yield preparation of high-electronic-quality graphene by a Langmuir–Schaefer approach. Small 2010;6(1):35–9.

[34] Khan U, O'Neill A, Lotya M, De S, Coleman JN. High-concentration solvent exfoliation of graphene. Small 2010;6(7):864–71.

[35] Shih C-J, Lin S, Strano MS, Blankschtein D. Understanding the stabilization of liquid-phase-exfoliated graphene in polar solvents: molecular dynamics simulations and kinetic theory of colloid aggregation. J Am Chem Soc 2010;132(41):14638–48.

[36] Anderson LR, Liu K-C. Pyrrole and pyrrole derivatives. Kirk–Othmer encyclopedia of chemical technology. John Wiley & Sons, Inc.; 2000. p. 16.

[37] Khan U, O'Neill A, Porwal H, May P, Nawaz K, Coleman JN. Size selection of dispersed, exfoliated graphene flakes by controlled centrifugation. Carbon 2012;50(2):470–5.

[38] Troitsky VI, Berzina TS, Fontana MP. Deposition of uniform conductive polyaniline films and approach for their patterning. Synth Met 2002;129(1):39–46.

[39] Paddeu S, Ram MK, Carrara S, Nicolini C. Langmuir–Schaefer films of a poly(o-anisidine) conducting polymer for sensors and displays. Nanotechnology 1998;9(3):228.

[40] Gaines GL. Insoluble monolayers at liquid–gas interfaces. New York: Interscience Publishers; 1966.

[41] Petty MC. Langmuir–Blodgett films: an introduction. Cambridge; New York: Cambridge University Press; 1996.

[42] Ebbing DD, Gammon SD. General Chemistry. Boston: Houghton Mifflin Co.; 2002.

[43] Hansen CM. Hansen solubility parameters: a user's handbook. Boca Raton, Fla.: CRC Press; 2000.

[44] De S, King PJ, Lyons PE, Khan U, Coleman JN. Size effects and the problem with percolation in nanostructured transparent conductors. ACS Nano 2010;4(12):7064–72.

[45] Nirmalraj PN, Lutz T, Kumar S, Duesberg GS, Boland JJ. Nanoscale mapping of electrical resistivity and connectivity in graphene strips and networks. Nano Lett 2010;11(1):16–22.

[46] Biswas S, Drzal LT. A novel approach to create a highly ordered monolayer film of graphene nanosheets at the the liquid–liquid interface. Nano Lett 2009;9(1):167–72.